We are Nitinol.™

Finite Element Analysis and Experimental Evaluation of Superelastic Nitinol Stents

Gong, Pelton, Duerig, Rebelo, Perry

Proceedings of SMST-2003
Monterey, CA
(eds.) T.W. Duerig, A. Pelton

2003

FINITE ELEMENT ANALYSIS AND EXPERIMENTAL EVALUATION OF SUPERELASTIC NITINOL STENT

Xiao-Yan Gong*, Alan R. Pelton*, Tom W. Duerig*,
Nuno Rebelo and Ken Perry*****

**Nitinol Devices & Components, 47533 Westinghouse Drive, Fremont, CA 94539 USA*
***ABAQUS West, 39221 Paseo Padre Parkway, #F, Fremont, CA, 94538 USA*
****ECHOBIO, 579 Azalea Avenue NE, Bainbridge Island, WA 98110*

ABSTRACT

The mechanical properties of Nitinol stents are normally evaluated experimentally due to complexities resulting from large deformations and material nonlinearity. Despite the difficulties associated with Finite Element Analysis (FEA), the success of the computational analysis in combination with experimental study leads to better understanding of stent performance. This paper presents comparisons between experimentally evaluated radial resistive forces of a Nitinol stent to predictions based on nonlinear FEA. The FEA was performed using ABAQUS with two user material subroutines independently developed specifically for Nitinol. Good agreements between the FEA and the experiments are shown for both user material subroutines.

KEYWORDS

NiTi, finite element analysis, superelastic, crush, stent, radial force.

INTRODUCTION

Recently, FEA on Nitinol has been improved to cover the superelastic behavior and has been proven to be a successful prediction tool in device design [1-6]. Among the many successful applications, Nitinol self-expanding stents have drawn much attention. Compared to a balloon-expandable stent, a Nitinol self-expanding stent provides constant gentle outwards pressure yet maintains high resistance to inward pressure and high crush resistance in addition to its ease of deployment [7-8]. Because of these unique properties, demands of Nitinol self-expanding stents are increasing for certain applications.

The most important mechanical requirements for a stent are radial force and fatigue life. Although both requirements can be evaluated through physical tests, they require "build-test" iterations and involve long time fatigue testing. Thus, they can be very costly and time consuming. A ten-year device fatigue life under the heart rate of 75 beats per minute projects a 400 million cyclic pulsatile loading on the stent. Even with an accelerated fatigue test, a 400 million-cycle fatigue test can last months. FEA is an extremely useful complement and has proven to be more effective and capable of providing a better and a more detailed understanding for fatigue and design [9-10].

This paper discusses the results using two different approaches to model the superelastic constitutive behavior of Nitinol. Both approaches are then used in the analysis to determine the radial force and crush characteristics of a Nitinol self-expanding stent. Comparisons with the corresponding tests confirm that FEA provides good predictions of the stent's mechanical response. Good agreement between two different constitutive approaches indicates FEA is a capable predictive tool in the early design phase of Nitinol devices.

CONSTITUTIVE MODELS

It is well known that Nitinol is a thermo-mechanical coupled material. Pelton et al (2000) demonstrated this thermo-mechanical coupled material response systematically [11]. In their work, uniaxial stress-strain behavior of Nitinol wires was studied from -100^{o}C to 150^{o}C as shown in Figure 1. The series of stress-strain responses at different temperatures demonstrate the highly nonlinear, path and temperature dependent material constitutive behavior.

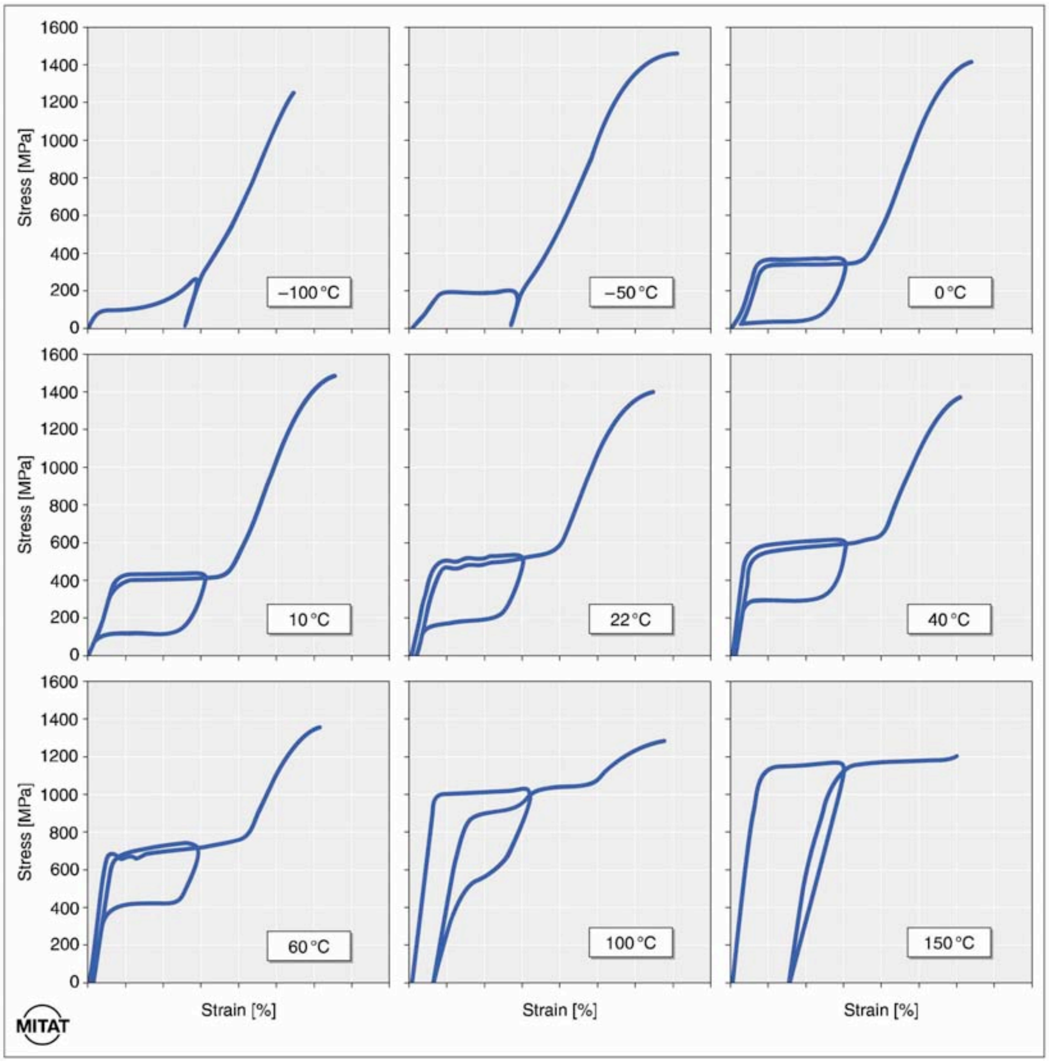

Figure 1. Uniaxial stress-strain relation at different temperatures

Pelton et al (1994) were also the first to address the nonlinear material behavior of Nitinol by taking advantages of the hyperelastic theory for rubbers [12]. This approach is very intuitive, as Nitinol is, to some extent, a "rubber in the metal form." Despite their success, hyperelastic theory is known to have stability issues that require more calibration tests (namely uniaxial tension, biaxial tension and shear) to stabilize the model. Furthermore, the hyperelastic material model does not address the path and temperature dependent material behavior of Nitinol [13].

Over the last ten years, many theories that account for the nonlinear path dependent thermo-mechanical constitutive behaviors applicable to Nitinol have been independently developed [14-18]. They build up the foundation for the state-of-art constitutive description of Nitinol. To date, advanced FEA of Nitinol has adopted those theories. The constitutive models used in this paper are based on the approaches proposed by Auricchio et al, and Qidwai and Lagoudas [16-18]. For completeness, their approaches are briefly summarized below.

Auricchio's approach is based on the generalized plasticity theory [16-17]. It models the superelastic behavior of Nitinol, where any strain increment is decomposed into a linear elastic part, and into a stress induced transformation part. The transformation part follows standard plasticity rules, such that strain increments can be derived from a plastic potential. The model includes transformation surfaces (analogous to yield surfaces) for both the austenite-to-martensite transformation and the reverse martensite-to-austenite transformation. The ABAQUS implementation allows for different elastic properties for austenite and for martensite, as well as different transformation stresses in tension and in compression. The loading can be either mechanical or thermal, and the transformation stresses (surfaces) are temperature dependent.

Qidwai and Lagoudas have developed constitutive models for shape memory and superelastic materials based on first principles [18]. In their approach, the second law of thermodynamics is written in terms of the Gibbs free energy. Strain, temperature and martensite volume fraction become state variables that must satisfy the second law of thermodynamics. An evolution equation for the martensite volume fraction is derived from a dissipation potential and the effective transformation surfaces are evaluated as functions of the state variables. This approach also allows for different temperature dependant elastic properties for austenite and martensite and accommodates both mechanical and thermal loading.

Both constitutive models need calibration based on uniaxial tensile test. Figure 2 plots the comparison of the two independently developed constitutive models and the experimental result of Nitinol tubing that has been processed to achieve an Af of 29^{o}C and is tested at 37^{o}C. Note that both models can be calibrated to predict the material's response well up to close to 8% strain based on a limited numbers of parameters. Discrepancy arises at higher strains because neither material model covers the plasticity in the martensitic phase. ABAQUS/Standard version 6.2-1 along with Nitinol UMAT/3D 3.24 developed by ABAQUS West and another User-defined material subroutine by EchoBio were used in the analyses.

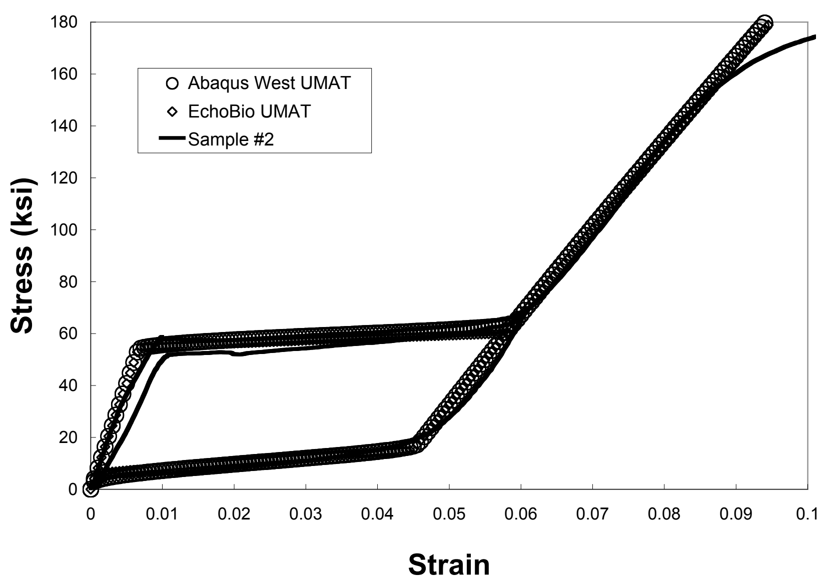

Figure 2. Comparison of FEA predictions and the experimental data

RESULTS AND DISCUSSIONS

RRF AND COF

RRF (Radial Resistive Force) and COF (Chronic Outwards Force) are important mechanical responses unique to Nitinol Superelastic stents. RRF is the force generated by a stent to resist the reduction in its diameter and COF is the force generated by a stent when it is self-expanded from a smaller diameter towards a larger diameter. Figure 3 illustrates schematically how these values are experimentally evaluated. Generally, this experiment is performed on a MTS system with customized test fixtures. The test is performed in a hot water bath so that a constant testing temperature of 37C is maintained. In the first step, the stent is crimped down to a small diameter in order to fit into the intended delivery system at a low temperature. Then, it is placed inside the Mylar loop with one end of the loop fixed to the test fixture and another end connected to the MTS force actuator. The hot water is then added so that the crimped stent is submerged and this causes the stent intended to expand back to its manufactured larger diameters. The Mylar loop is now a constraint against the self-expansion of the Nitinol stent. The Mylar loop experiences a radial expansion force that is transferred to the load cell as a pulling force. By moving the MTS actuator down, one can release the pulling force and record the force as function of the actuator displacement. The stent diameter change can be calculated based on the actuator displacement. Thus, the force as a function of the stent diameter is obtained in this way. Notice that this records the force as the stent is released from its crimped diameter; therefore, the measured force corresponds to the COF. At a given stent diameter, when RRF is of interest, the MTS head is reversed to move up so that a pulling force on the Mylar is transferred to the stent as a radial compression. By crimping down the stent to a smaller diameter, one can obtain the RRF. After the RRF is obtained, one can reverse the MTS actuator again to complete the test or can repeat the sequences to obtain the RRF at different stent diameters.

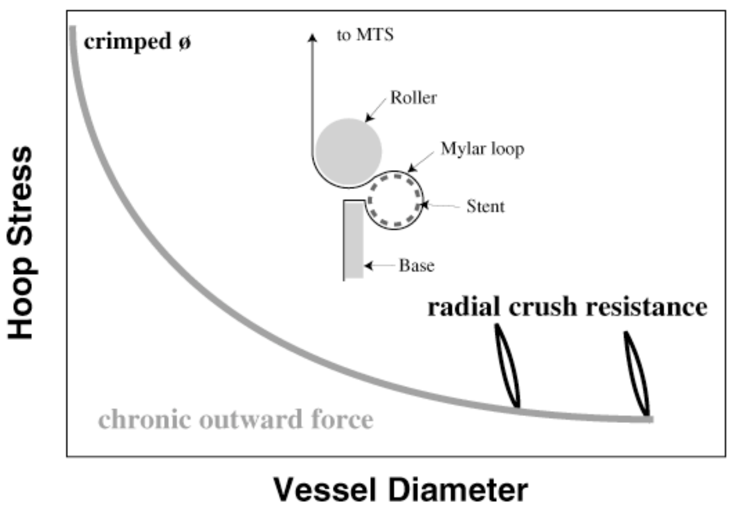

Figure 3. Schematic radial force test set up

For simplicity, a two-strut model shown in Figure 4 is used in our FEA. For comparison purposes, the same model and mesh were used in the study. A 10mm SMART Control[TM] stent from Cordis self-expanding stent product line is selected for the RRF and COF study. In this model, symmetrical boundary conditions are applied to the open surfaces to maintain symmetrical deformation. User-defined rigid surfaces are used to compress and release the stent to the necessary stent diameters. Artificial stability option in ABAQUS/Standard is also turned on so that the analysis can run smoothly. The total strain energy and total artificial strain are traced during the whole simulation to ensure that the artificial energy is negligible.

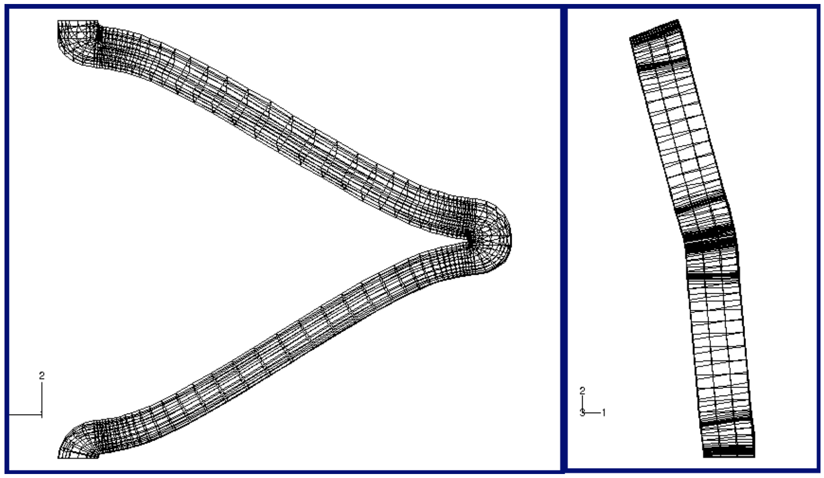

Figure 4. Side (left) and top (right) views of a two strut model

Figure 5 shows the comparison between the FEA predictions and the test result. In either material constitutive model, the re-load of the Nitinol is not simulated correctly. In addition, there are discrepancies at smaller stent diameters. This corresponds to the lack of a plasticity model at high strain in the martensitic phase in both material models; however, the COF agrees well with the experimental result at larger diameters. Luckily, larger diameters are of greater interests in stent applications. Furthermore, if one keeps in mind that RRF originates from the material response on the loading path, one can find the correct predictions of the RRF from the FEA results during the compression of the stent. Thus, even for these challenging results, the FEA solution agrees well with the experimental results.

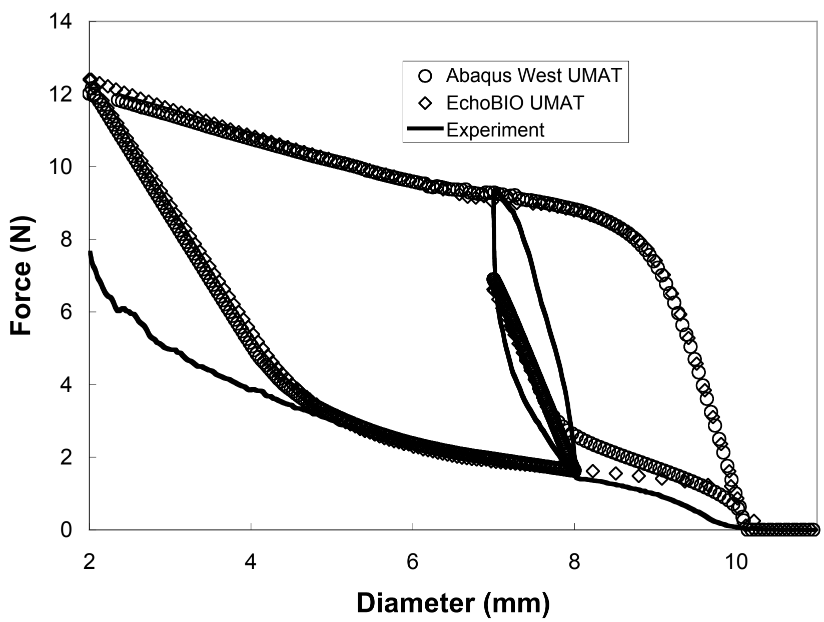

Figure 5. Comparisons of FEA predictions and the tests results

Figure 6 shows the strain contours on the deformed struts. The high strain locations identify the fatigue critical areas in stent manufacturing. Figure 7 plots the comparison of peak maximum principal strains for both material models. There is a good agreement between both material models and actual material behavior.

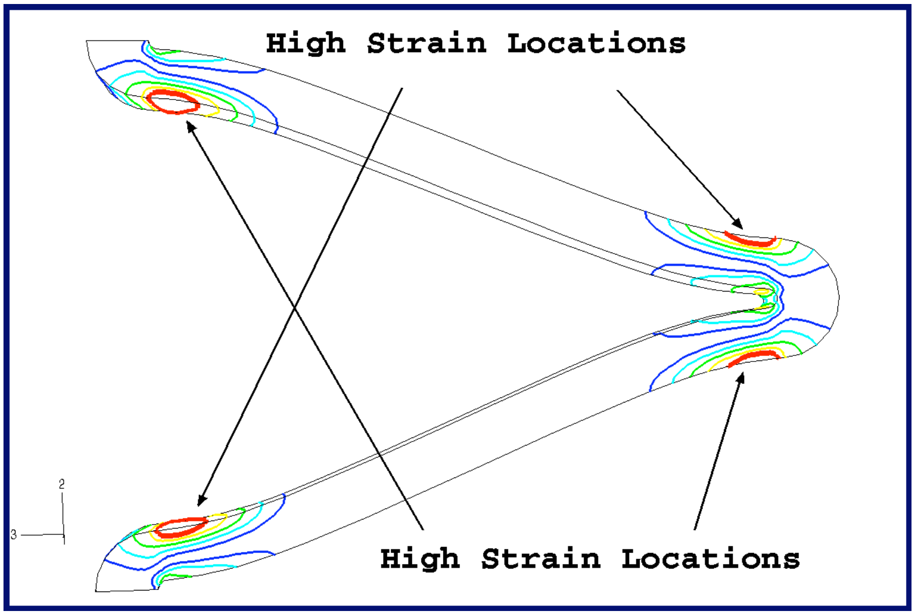

Figure 6. Maximum principal strain contours indicate the fatigue critical areas

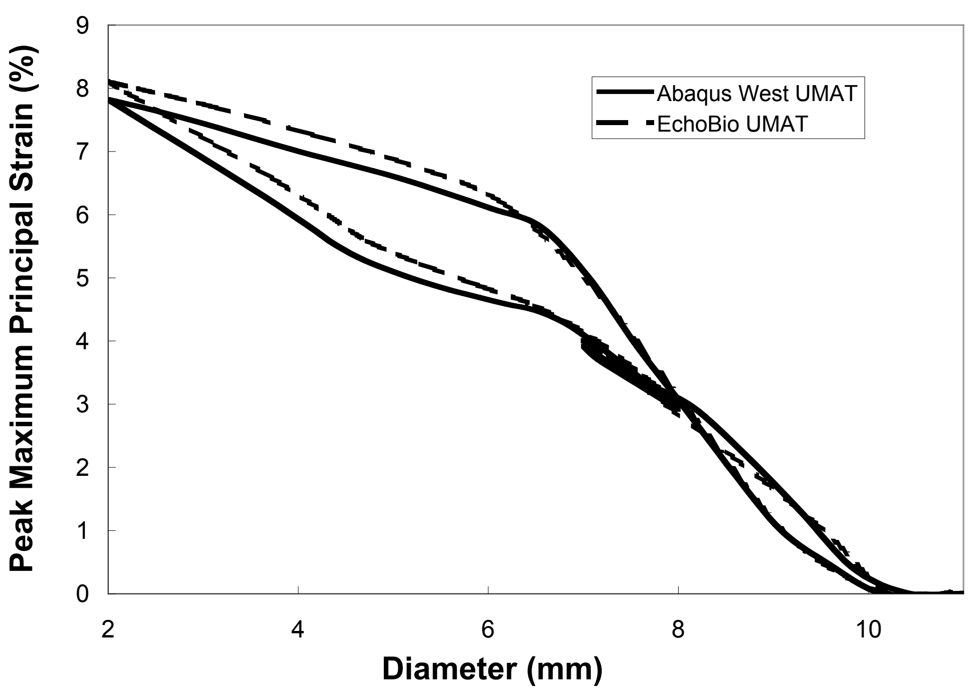

Figure 7. Peak maximum principal strain as function of stent diameter

CRUSH RESISTANCE

The same diameter stent was chosen for crush test. The crush test was performed on EnduraTec desktop tester ELF/3200 series capable of higher displacement and load resolution. The test setup is straightforward, first the stent was deployed inside a 8mm ID 5% compliant tube (over 100mmHg pressure differential) to simulate the worst case oversizing per the product IFU. The stented tube is then crushed between two rigid plates and the force and displacement were monitored. Air heating is used in this test. Environment temperature is 37°C to simulate the body temperature.

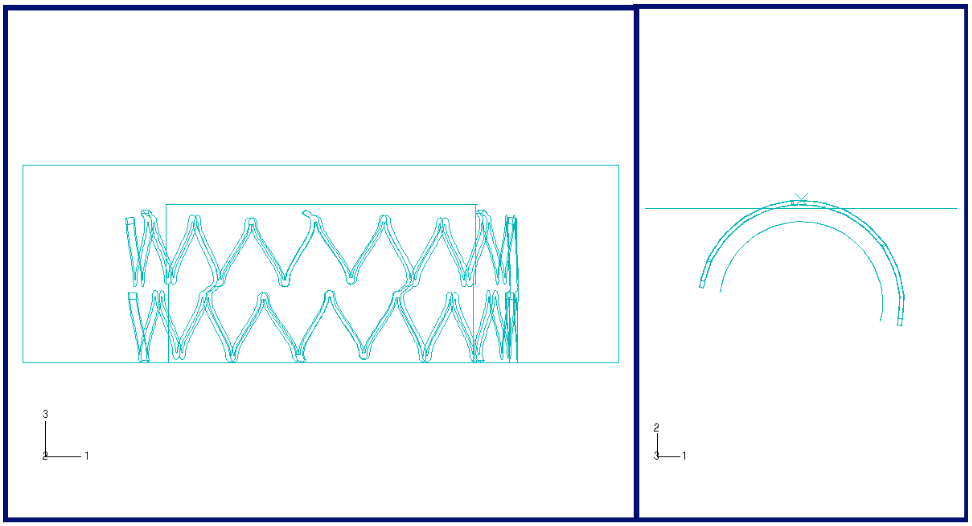

Figure 8. Side (left) and top (right) views of the FEA model for crush simulation

Figure 8 shows the FEA model for this simulation. Due to the repetitive patterns of a stent, only two half-row struts are used in the analysis. Axial and rotational repetitive boundary conditions are applied to the open ends of the model. The analysis involves rigid-to-flexible and flexible-to-flexible contacts over three steps. In the first step, all the contacts are removed so that the compliant tube, simulated as shell elements, is pressurized to expand to a diameter slightly larger than the stent OD. In the second step, the contact between the compliant tube and the stent OD is activated and the pressure acting on the tube ID is released completely so that the tube and stent reach their equilibrium positions. In the last step, contact between a rigid surface and the tube OD is activated so that the rigid surface can crush the stented tube. This simulation is difficult, not only due to the contacts and the material nonlinearity, but mainly because of the buckling of the stent. As a matter of fact, the buckling is visually observed both from the test and the FEA as shown in the comparison of the deformed shapes from the experiment and the FEA in Figure 9.

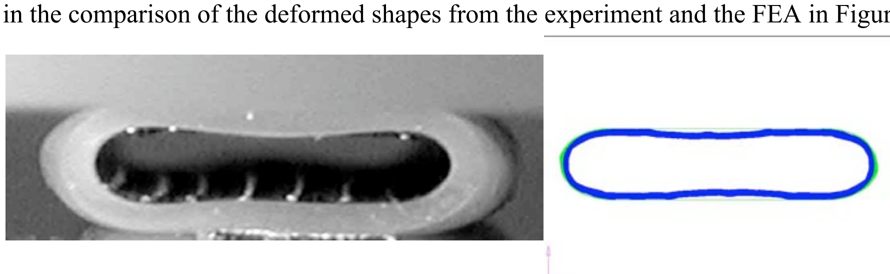

Figure 9. Comparison of deformed stent shape from experiment (left) and FEA (right)

Figure 10 plots the force-displacement response when the stented tube is crushed. Once again, good agreement between the FEA and the experiment indicates that both the material models represent the material response well. Figure 11 compares the peak maximum principal strain as function of the crush displacement for both material models. Once again, they agree well.

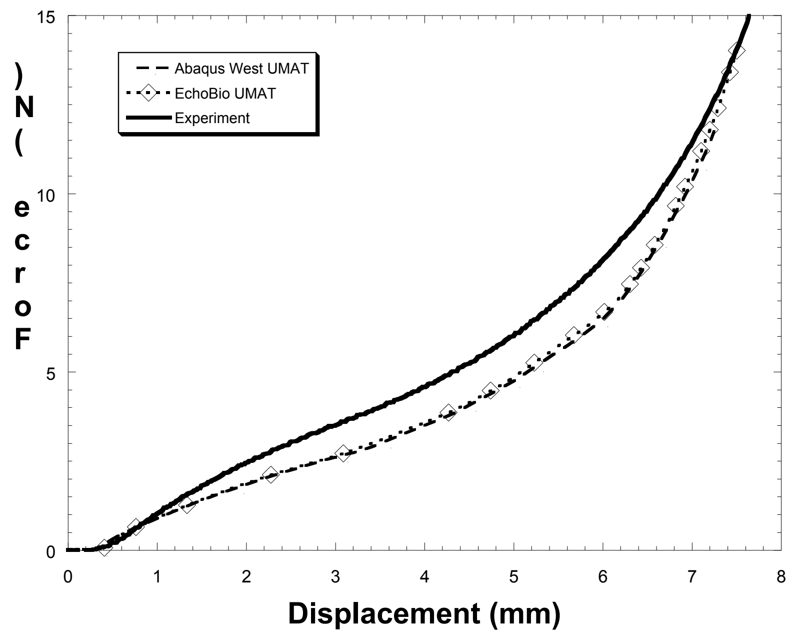

Figure 10. Comparison of force-displacement relations from experiment and FEA

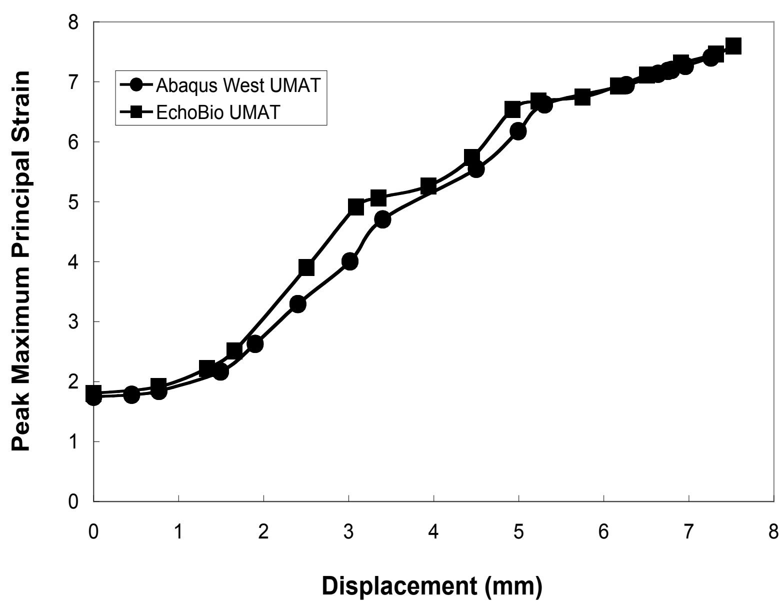

Figure 11. Peak maximum principal strain as function of displacement from two different material models

CONCLUSIONS

We showed that FEA based on two different user-defined material subroutines predicts consistently mechanical response for stents. Key results from FEA done with both material models agree well with experimental results, indicating that FEA is a powerful predictive tool that can be used in product development and design. Improvement of the material constitutive models for Nitinol is necessary to accurately describe the plasticity in the martensitic phase as well as under multiple loading and unloading sequences.

REFERENCES

1. X. Gong and A. R. Pelton, ABAQUS Analysis on Nitinol Medical Applications, Proceedings of ABAQUS Users' Conference, New Port, Rhode Island, 2002, p. 1.
2. N. Rebelo and M. Perry, Finite Element Analysis for the Design of Nitinol Medical Devices, Min. Invas. Ther. & Allied. Technol., 9 (2) 2000, p. 75.
3. N. Rebelo, M. Hsu and Foadian, H., Simulation of Superelastic Alloys Behavior with ABAQUS, in SMST-2000: Proceedings of the International Conference on Shape Memory and Superelastic Technologies (S.M. Russell and A.R. Pelton eds.), Pacific Grove, California, USA, 2000, p. 495.
4. E. Patoor, Y. Gillett, E. Segard and M. Berveiller, Optimisation of Superelastic Elements, in SMST-97: Proceedings of the Second International Conference on Shape Memory and Superelastic Technologies, (A.R. Pelton, D. Hodgson, S. Russell and T.W. Duerig eds.), Pacific Grove, California, USA, 1997, p. 35.
5. F. Trochu and P. Terriault, Finite Element Stress Analysis of A Shape Memory Medical Stent, in SMST-97: Proceedings of the Second International Conference on Shape Memory and Superelastic Technologies, (A.R. Pelton, D. Hodgson, S. Russell and T.W. Duerig eds.), Pacific Grove, California, USA, 1997, p. 595.
6. M. D. Perry and R.T. Chang, Finite Element Analysis of NiTi Alloy Stent Deployment, in SMST-97: Proceedings of the Second International Conference on Shape Memory and Superelastic Technologies, (A.R. Pelton, D. Hodgson, S. Russell and T.W. Duerig eds.), Pacific Grove, California, USA, 1997, p. 601.
7. T. W. Duerig and M. Wholey, A Comparison of Balloon- and Self-Expanding Stents, Min. Invas. Ther. & Allied. Technol., 11 (4) 2002, p. 173.
8. T. Duerig, D. E. Tolomeo, and M. Wholey, An Overview of Superelastic Stent Design, Min. Invas. Ther. & Allied. Technol., 9 (3/4) 2000, p. 235.
9. D. Tolomeo, S. Davidson and M. Santinoranont, Cyclic Properties of Superelastic Nitinol: Design Implications, in SMST-2000: Proceedings of the International Conference on Shape Memory and Superelastic Technologies (S.M. Russell and A.R. Pelton eds.), Pacific Grove, California, USA, 2000, p. 471.
10. C. Kugler, D. Maston and K. Perry, None-Zero Mean Fatigue Test Protocol for NiTi, in SMST-2000: Proceedings of the International Conference on Shape Memory and Superelastic Technologies (S.M. Russell and A.R. Pelton eds.), Pacific Grove, California, USA, 2000, p. 409.
11. A. R. Pelton, J. Dicello and S. Miyazaki, Optimisation of Processing and Properties of Medical Grade Nitinol Wire, Min. Invas. Ther. & Allied. Technol., 9 (2) 2000, p. 107.
12. A. R. Pelton, N. Rebelo, T.W. Duerig and A. Wick, Experimental and FEM Analysis of the Bending Behavior of Superelastic Tubing, in SMST-94: Proceedings of the First International Conference on Shape Memory and Superelastic Technologies, (A.R. Pelton, D. Hodgson and T.W. Duerig eds.) Pacific Grove, California, USA, 1994, p. 353.
13. M. Pease and B. Walsh, Nitinol Constitutive Law Comparison for Finite-Element Analysis, in SMST-2000: Proceedings of the International Conference on Shape Memory and Superelastic Technologies (S.M. Russell and A.R. Pelton eds.), Pacific Grove, California, USA, 2000, p. 495.
14. R. Abeyaratne and J. Knowles, A Continuum Model for A Thermoelastic Solid Capable of Undergoing Phase Transitions, J. Mech. Phys. Solids, 41, 1993, p 541.
15. L. Anand and M. Kothari, A Computational Procedure for Rate-Independent Crystal Plasticity, J. Mech. Phys. Solids, 44, 1996, p525.

16. F. Auricchio and R. Taylor, Shape Memory Alloys: Modeling and Numerical Simulations of the Finite-Strain Superelastic Behavior, Comput. Methods. Appl. Mech. Engng. 143, 1996, p175.
17. F. Auricchio and R. Taylor, Shape Memory Alloys: Micromodeling and Numerical Simulations of the Superelastic Behavior, Comput. Methods. Appl. Mech. Eng. 146, 1997, p281.
18. M. A. Qidwai and D .C. Lagoudas, Numerical Implementation of A Shape Memory Alloy Thermomechanical Constitutive Model Using Return Mapping Algorithms, Int. J. Numer. Meth. Engng. 46, 2000, p1123.